Journal of Spacecraft and Rockets

VOLUME 8 APRIL 1971 NUMBER 4

Electrostatic Ion Thruster ESKA-18-P of the DFVLR

SIEGFRIED F. J. BAUMGARTH,* HARRO A. W. BESSLING,† AND UWE W. SPRENGEL‡
Institute for Electric Propulsion and Power Supply, DFVLR, Braunschweig, West Germany

Related to an electric propulsion system capable of spiraling a satellite from a parking orbit into the synchronous orbit, the ion-thruster ESKA-18-P has been designed for an electric input power of about 700w and an exhaust velocity of 38 km/sec. The characteristic data of this mercury thruster are presented as function of the magnetic field and different mass flow ratios. In addition, some experimental results on hollow cathodes obtained in separate investigations, and beam diagnostic measurements with a multiple Faraday-probe, are reported. Finally, the application of the thruster for a solar electric propulsion module of 2.5 kw is demonstrated.

Introduction

IN the Federal Republic of Germany, project studies of a solar electric propulsion module, called SELAM,[1,2] have been done for 2.5 kw of electric power. This would be the first step of testing German ion thrusters in space. Increasing the electric power, Europe would be able to raise the payload capability of its launchers for the synchronous orbit by a factor of three.[3] According to orbit transfer calculations[4,5] an optimum exhaust velocity of about 40 km/sec, depending on the power supply, has to be realized. Because of the given power input of 2.5 kw, a thruster of about 700w has been investigated, considering a cluster of three thrusters, before continuing research on the 30-cm ion thruster.[6] Related to the exhaust velocity corresponding to 1.5 kv of positive high voltage, an ion current of 0.35 amp is required, resulting in a beam diameter of 18 cm.

Figure 1 shows a cut-away view of the thruster[7,8] with separated tanks for the main propellant feed system with mercury as propellant and for the plasma bridge neutralizer. The mercury tank is sized for 200 days of operation. A porous tungsten diaphragm in the vaporizer separates the liquid and vapor phases of the Hg propellant. Passing the isolator, which is necessary in the case of clustering using one tank only, the mercury is fed through the hollow cathode or through the distributor into the discharge chamber, where the propellant is ionized by electron bombardment. The ions are extracted by the accelerating system of two molybdenum grids with 4-mm-diam holes. The buckling of the grids, separated by 1.5 mm, is prevented by a special mounting support. The grids are allowed to expand in the radial direction only, without bending at the point of mounting. A plasma bridge neutralizer emits the electrons into the ion beam. A Faraday cage around the ion source prevents arcing outside the thruster. The thruster is tested in a vacuum facility (with prechamber) of 2 m in diameter and 5 m in length at a pressure of 10^{-7} to 10^{-6} torr (liquid-nitrogen cooled). The tests with the prototype ESKA-18-P have been performed since fall 1969.

The control system of the thruster controlling the vaporizer is based on the ion beam current or the discharge current. If the ion beam is increasing, too much propellant is fed to the thruster, and the power of the vaporizer must be decreased. In this kind of operation no lifetime problems of the vaporizer will occur, but the porous tungsten diaphragm will change the mass flow rate over a long time. Life problems of the main cathode can be eliminated in certain limits by controlling the discharge current with respect to an ideal discharge characteristic given by a function generator. The same control system is used for the plasma bridge neutralizer taking the keeper current as control element for the neutralization cathode. One control system has been in operation since January 1970 and is based on pulse-width modulators.[9]

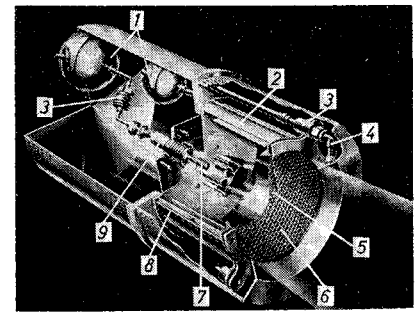

Fig. 1 Cut-away view of the electrostatic ion thruster "ESKA", 1) = Hg tanks, 2) = anode, 3) = vaporizer, 4) = neutralizer, 5) = screen, 6) = accelerator, 7) = hollow cathode, 8) = bar magnet, and 9) = isolator.

Presented as Paper 70-1101 at the AIAA 8th Electric Propulsion Conference, Stanford, California, August 31–September 2, 1970; submitted October 10, 1970; revision received December 14, 1970. Sponsored by the Bundesministerium für Bildung und Wissenschaft under contract RFF 3046.

* Diplom Physics.
† Research Physicist
‡ Diplom Engineer

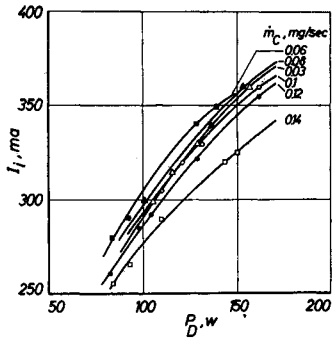

Fig. 2 Ion beam current I_i vs discharge power P_D, including the cathode power, at a constant total mass flow rate $\dot{m}_p$ of 0.78 mg/sec; V_{pos} = 1.5 kv, and V_{neg} = 1.0 kv.

Measurements

Discharge

The loss energy of ion thrusters is defined as

W_T = sum of all loss powers/ion beam current (ev/ion) (1)

where the loss powers are those for the mercury feed system, the main cathode, the discharge, accelerator and neutralizer. From this value, it is easy to calculate the energy efficiency defined as

η_e = ion beam power (directed kinetic energy)/ total electric power input (2)

If V_{pos} is the voltage required for the exhaust velocity, then

$$\eta_e = V_{pos}/(W_T + V_{pos}) \quad (3)$$

The main losses are inside the discharge chamber, including the discharge power and cathode power. Therefore another loss energy is defined:

W_D = discharge power including cathode power/ ion beam current (ev/ion) (4)

Theoretically W_D would be 10.4 ev/ion, in practice, however, the discharge loss energy is in the range of some hundred ev/ion.

The problem of the ionization in the discharge chamber consists in distributing the ionization collisions homogeneously over the total discharge volume, or, better, close to the grid area. Concentrating the ionization processes close to the center, the possibility of recombination in this area would increase. In this case, neutral particles in the outside region will leave the discharge chamber. Two methods will be applied to prevent such concentration of ionizations: feeding the neutral particles in the correct point into the discharge chamber and having the suitable magnetic field corresponding to the thruster geometry.

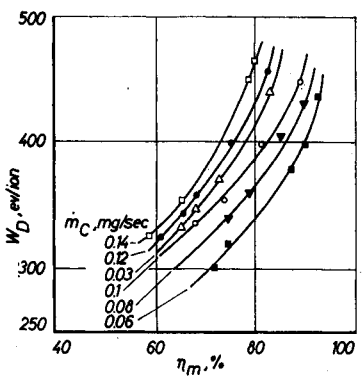

Fig. 3 Discharge loss energy W_D vs mass utilization factor η_m (same $\dot{m}_p$, V_{pos}, V_{neg} as Fig. 2).

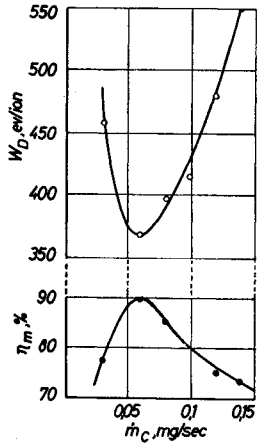

Fig. 4 Discharge loss energy W_D at η_m = 85%, and η_m at W_D = 400 ev/ion, vs cathode mass flow rate (same $\dot{m}_p$, V_{pos}, V_{neg} as Fig. 3.).

Injecting the propellant mainly through the hollow cathode of the discharge, a very high concentration of neutral particles close to the cathode tip would result. Thus a high ionization collision rate appears in a small region because of the large number of primary electrons and of neutral particles. Further, outside of this area, Maxwellian electrons are present mainly and because of the necessary diffusion of the ions a high recombination rate is caused. Therefore it is useful to feed the main propellant separated from the electron injection. Only a small fraction has to flow through the hollow cathode in order to maintain the plasma bridge for the electrons. The main mercury flows into the discharge chamber close to the anode.

In order to determine the optimum ratio of the mass flow rates through the cathode and through the distributor, two vaporizers have been used at a constant magnetic field. Figure 2 shows ion beam current I_i vs discharge power P_D for various values of mass flow rate through the cathode $\dot{m}_c$, with total mass flow held constant at 0.78 mg/sec. The ion beam current increases with smaller $\dot{m}_c$. However, below 0.06 mg/sec it decreases again. The W_D's calculated from Fig. 2 are plotted in Fig. 3 as a function of mass utilization factor η_m. Further cross plotting gives W_D vs $\dot{m}_c$ at η_m = 85% and η_m vs $\dot{m}_c$ at W_D = 400 ev/ion as shown in Fig. 4. The decreasing $\dot{m}_c$ agrees with the model previously assumed. The increase of W_D below the optimum $\dot{m}_c$ of 0.06 mg/sec can be explained by the decreasing primary electron current. The electrical conductivity of the plasma bridge to the discharge decreases, lowering the primary electron current necessary for the optimum ionization.[10,11]

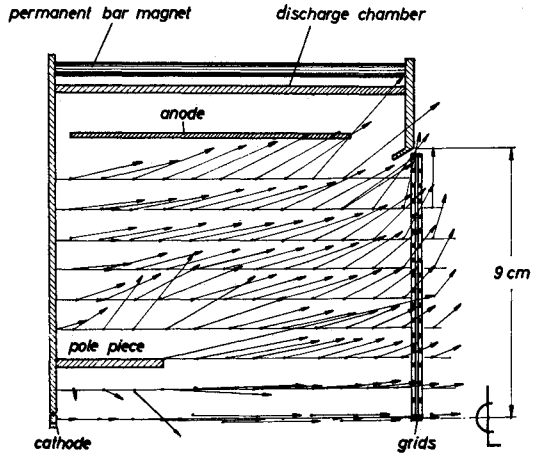

Fig. 5 Distribution of the magnetic induction; 1cm = 10 Gauss, 12 permanent magnets.

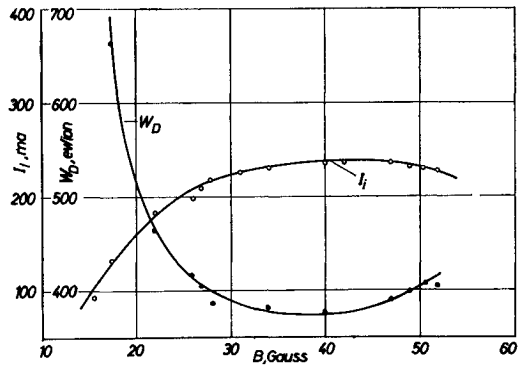

Fig. 6 I_i and W_D vs magnetic induction B at constant $\dot{m}_p$ of 0.58 mg sec; V_{pos} = 1.5 kv and V_{neg} = 1.0 kv.

The magnetic field also has to be optimized. The magnetic field configuration of ESKA-18-P is shown in Fig. 5. Keeping this configuration, the magnitude of the magnetic induction was varied by replacing the permanent bar magnets by electromagnets of the same shape. Figure 6 shows the resulting curves of I_i and W_D vs the magnetic induction at a constant mass flow rate. The I_i in this special case is relatively small, because the discharge current at low magnetic inductions increases very much.

At normal mass flow rates the discharge current exceeds the present capability of the discharge power supply. In the range of 35 to 45 Gauss the ion beam current and the discharge loss energy are nearly constant. This optimum represents the best primary electron distribution within the discharge chamber.

Hollow Cathode

In ESKA-18-P a hollow cathode[12,13] is used as discharge cathode and plasma bridge neutralizer.[14] In the following, the mechanism of the keeper-cathode-system and the possibility of using the keeper as control element are investigated. Furthermore, a relation between the mass of the power supply and propellant mass of the neutralizer system depending on the discharge mode is shown. A hollow cathode operates in two different modes, the spot mode and the plume mode. For the change from spot mode to plume mode the following condition has to be satisfied[15]:

$$j_e/j_i \geqq [(m_i/m_e)^{1/2}\lambda_e/\lambda_i]^{1/2} \approx 40 \qquad (5)$$

where $j_{e,i}$ = current density of electrons or ions, $\lambda_{e,i}$ = mean free path of electrons or ions, and $m_{e,i}$ = mass of an electron or ion.

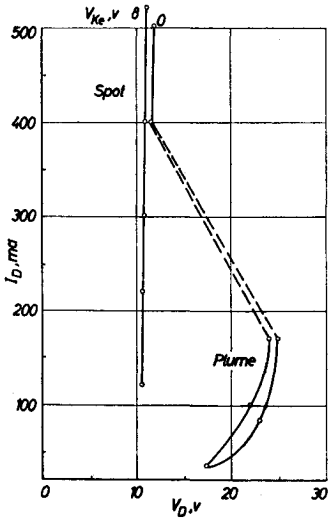

Fig. 7 Discharge current I_D vs discharge voltage V_D at constant $\dot{m}_p$ of 0.1 mg/sec.

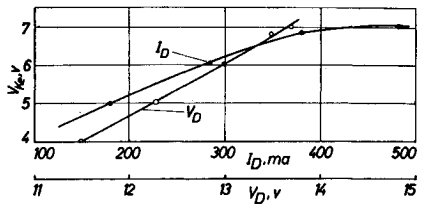

Fig. 8 Keeper voltage V_{Ke} vs I_D and V_D for the spot mode at $\dot{m}_p$ = 0.4 mg/sec.

Introducing the space charge instead of the current density, the change between modes evidently depends also on the positive and negative space charge in front of the cathode. The space charge can be influenced by the keeper. Connecting the keeper with the cathode including 1 kΩ, we get a positive current on the keeper consisting of ions moving to the keeper and electrons coming from the keeper into the discharge. The space charge in front of the cathode depends on this current. Applying a positive voltage to the keeper with respect to the cathode, we get a negative keeper current.

The discharge characteristics (I_D vs V_D) in Fig. 7 show the influence of the keeper potential V_{Ke} as parameter on the discharge mode. Both characteristics were obtained at a constant mass flow rate $\dot{m}_p = 10^{-4}$ g/sec. At V_{Ke} = +8v, the cathode is operating in the spot mode over the total range from I_D = 120 ma to I_D = 510 ma. When V_{Ke} = 0, the discharge changes to the plume mode for $I_D < 400$ ma, increasing V_D strongly.

Corresponding to Eq. (5), the change from spot to plume mode can be explained as follows: decreasing the discharge power the ionization degree is reduced. Therefore the fraction of the ion current in the ambipolar current and the positive space charge in front of the cathode decreases. At an applied V_{Ke} of 8 v this is not sufficient to change the mode because of the additional negative keeper current. However at zero external keeper voltage and positive keeper current the mode changes into plume mode. This change is only possible at $\dot{m}_p$ <0.1 mg/sec. The result of these experiments is the suitable choice of the keeper potential influencing the mode and stability of the discharge.

The following characteristics of the hollow cathode are given to show the possibility of using the keeper as the indicator for the control system of the neutralizer. In Fig. 8 the keeper voltage as a function of the discharge current and voltage is plotted for spot mode at $\dot{m}_p$ = 0.4 mg/sec. The characteristics of plume mode are shown in Fig. 9 at $\dot{m}_p$ = 0.01 mg/sec and the applied keeper voltage U_{KeP} as parameter.

Table 1 compares the spot and plume modes of the hollow cathode operating as neutralization cathode. The data include the loss energy for one electron, the propellant mass $\dot{m}_p$ for 6 months of operation and the additional mass for the power supply m_{ps}, assuming a specific mass of 30 kg/kw.

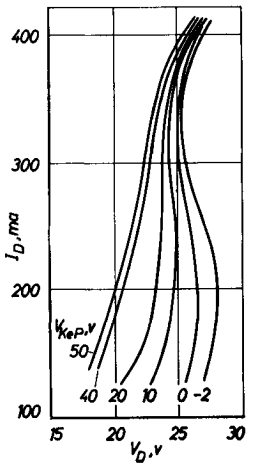

Fig. 9 Plume mode characteristics: I_D vs V_D at $\dot{m}_p$ = 0.01 mg/sec.

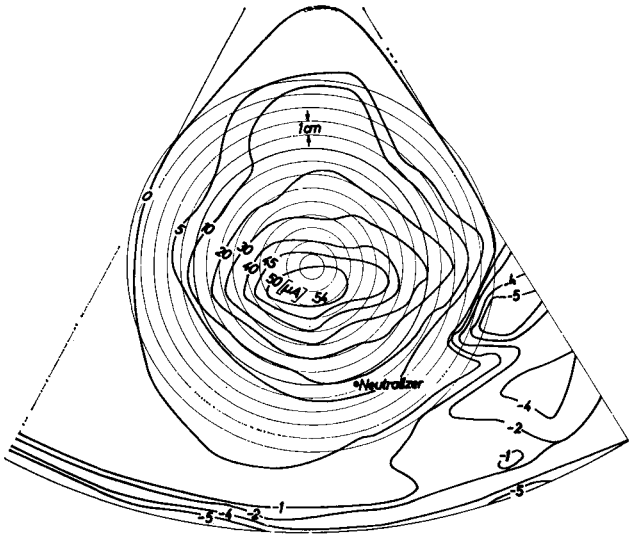

Fig. 10 Radial current distribution; spacing from the accelerator: 20 cm; total ion beam current 336 ma; fully neutralized.

The plume mode requires only 0.1 as much propellant, but 2.4 as much power. Accounting for the mass of the power supply, the plume mode operation for 6 months is better by a factor of 4.

Multiple Faraday-Probe

A multiple Faraday-probe was built, which can be swept through the beam and axially moved by means of a suitable mechanism. The axis of rotation of the probe is located 27 cm above the axis of the thruster. The total length of the probe with 17 single Faraday-cups spaced by 2.5 cm and insulated against each other is 47 cm. At present the maximum axial distance from the accelerator is 43 cm.

The single cups are connected with a selector switch, so that the reading of the measured cup currents occurs successively by one microammeter. Presently secondary electrons due to ion impact on the probe's surface are neglected. Therefore the cups have flat bottoms instead of conically shaped ones. According to Ref. 16, the secondary emission in electrons/ion for 2-kev mercury ions is less than 0.1 for stainless steel.

Figure 10 shows the results of using the probe (arm and Faraday-cups) at target potential (zero). Thus, the cup currents give only the difference current of electrons and ions. An asymmetric influence, resulting in an excess of electrons at the beam boundary nearest to the neutralizer, and a lack of electrons at the opposite side of the beam, disappears at more down-stream positions, demonstrated in Fig. 11. From both figures it is evident, that at these axial positions the ion beam is not yet neutralized in a sense that each ion pulls along an electron.

According to Fig. 10 it is assumed, that some electrons reach directly the Faraday-cups (zero potential) before

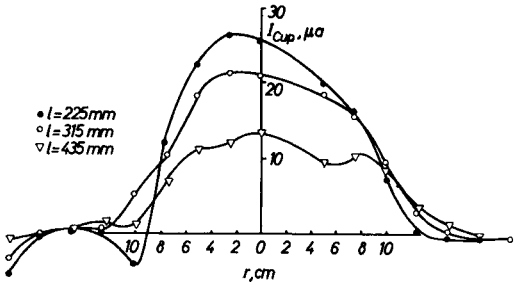

Fig. 11 Radial distribution of the cup current at different axial positions l; total ion beam current: 325 ma.

Table 1 Spot vs plume mode characteristics

	Spot	Plume
Discharge current, I_D, amp	0.5	0.5
Discharge voltage, U_D, v	12	29
Keeper voltage, V_{Ke}, v	10	20
Keeper current, I_{Ke}, amp	10^{-2}	10^{-2}
Propellant flow rate, $\dot{m}_p$, mg/sec	0.15	0.016
Discharge power, P_D, w	6	11.5
Keeper power, P_{Ke}, w	0.1	0.2
Total power, P, w	6.1	14.7
Propellant mass for 6 months, m_p, kg	2.35	0.25
Electron loss energy, W_e, ev/electron	12.2	29.4
Mass of power supply, m_{ps}, kg	0.18	0.44
$m_p + m_{ps}$, kg, for 6 months	2.54	0.6

entering the ion beam, because the potential difference between neutralizer and cups is greater than that between neutralizer and beam boundary. Thus, the excess of electrons near the neutralizer is certainly caused by direct electron impact on the Faraday-cups, so that the lack of electron current at the opposite side of the beam is resulting.

As Fig. 11 shows the relative maximum of beam current (ions and electrons) is shifted towards the neutralizer. But this is not necessarily a thrust misalignment, because the maximum of the ion beam might still be in the beam axis. At present measurements are done to achieve radial distributions of ion current, in order to learn more about a possible beam deflection due to the neutralizer and about beam spreading. Possibly two symmetrically arranged neutralizers are required to avoid this one-sided influence.

According to beam spreading first measurements indicate an angle of divergence of about 5°. However, these values have been evaluated from single ion beam profiles under the assumption of radial symmetry.

Characteristics of ESKA-18-P

The vaporizer feed pressure is ~2 atm. The vaporizer, made of molybdenum with an electron-beam-welded, porous tungsten diaphragm, needs 7 w_e of power (the mass flow is ~0.8 mg/sec), and it operates at ~270°C. The mercury vapor is fed through the isolator and the main hollow cathode into the discharge chamber. A main part is fed through the distributor. The cathode and isolator need 30 w_e. The discharge power, however, depends on $\dot{m}_p$ and is related to the desired ion beam current. The ion losses on the acceleration electrode depend strongly on η_m.

Operating near η_m = 85%, they are ~0.6% of the total ion beam. Taking the maximum value of 2 ma, the total power losses on the grid are 5 w, because of 1 kv negative and 1.5 kv positive high voltage. The neutralizer is operating

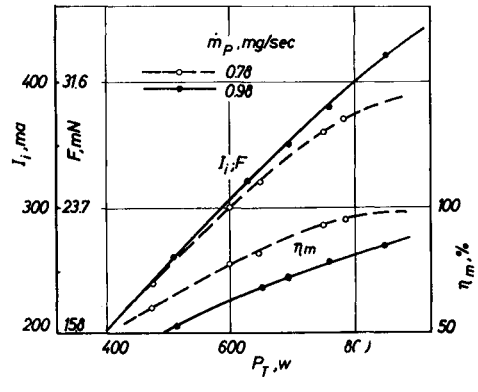

Fig. 12 Ion beam current I_i and thrust F vs total power input of the thruster P_T; V_{pos} = 1.5 kv and V_{neg} = 1.0 kv.

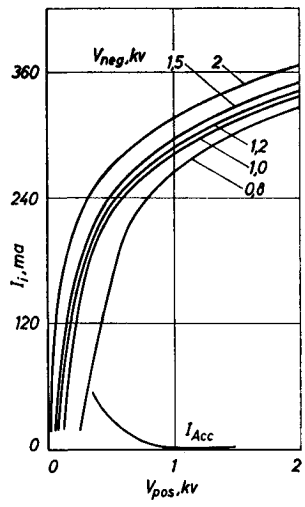

Fig. 13 I_i vs V_{pos} at $\dot{m}_p$ = 0.78 mg/sec and P_D = 120 w; accelerator current is indicated.

with a second mercury vaporizer, but because of its smaller mass flow rate and its location nearer the discharge chamber (radiation heat), only 3 w are needed. The hollow cathode operating as plasma bridge neutralizer needs 21 w_t. The keeper losses are negligible. Another problem is the potential of the neutralizer in order to control the electron flux equalizing the ion beam current. To get 300 ma of electron current we need 10 to 20 v, depending on the neutralizer mass flow rate. This takes up to 6 w of power losses. So the neutralizer needs up to 30 w of total electric power losses. For the calculation of the total thruster loss energy W_T (ev/ion), all the aforementioned losses (vaporizer, accelerator, neutralizer) have been kept constant at different mass flow rates and ion beam currents. The following diagrams give some data of the total thruster characteristics. In Fig. 12, I_i is plotted vs the total power input of the thruster P_T for two different $\dot{m}_p$'s. With V_{pos} = 1.5 kv, and V_{neg} = 1.0 kv, the required exhaust velocity of 38 km/sec was obtained. The diagram was obtained by varying V_D. A second scale gives the thrust F vs P_T. From these curves we get η_m vs P_T, which is included and scaled on the right ordinate.

The dependence of I_i on V_{pos} at P_D = 120 w and $\dot{m}_p$ = 0.98 mg/sec is plotted in Fig. 13. Because of the scale of the beam current the acceleration loss current is indicated only. The most interesting curve is shown in Fig. 14, where the thruster loss energy W_T is plotted vs η_m for $\dot{m}_p$ = 0.78 mg/sec. Below η_m = 60%, the curve is given as broken line, because this region is of no interest for a thruster.

Application of ESKA-18-P

Optimal design for a given mission is a question of time when the additional mass of the power supply Δm_{ps} will be comparable to the additional propellant mass. This is demonstrated in Fig. 15. At $\dot{m}_p$ = 0.8 mg/sec, 50 w_e are needed to produce an I_i of 190 ma. An additional 50 w produces 90 ma more, whereas a further increase of 50 w will raise I_i by only 40 ma. This is the same problem considered

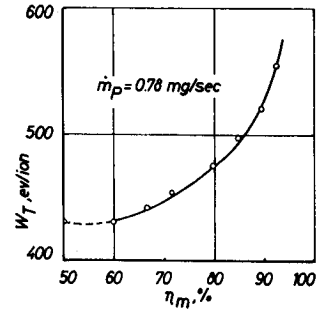

Fig. 14 Thruster loss energy W_T vs mass utilization factor η_m at $\dot{m}_p$ = 0.78 mg sec; V_{pos} = 1.5 kv, and V_{neg} = 1.0 kv.

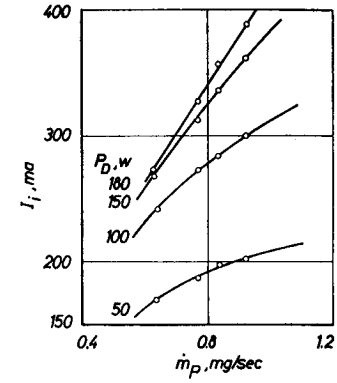

Fig. 15 I_i vs $\dot{m}_p$ at constant discharge power inputs.

already in the discussion of the operation of the plasma bridge neutralizer. At higher $\dot{m}_p$'s, less power is required. Therefore a very intensive mission analysis with an optimization of η_m and m_{ps} is necessary in order to know the optimum operation point of the thruster.

Considering again the solar electric propulsion module of 2.5 kw, three ESKA-18-P thrusters, each with about 700 w_e input can be operated. For redundancy,[17] 6 thrusters (with 3 in stand-by-mode) can be clustered in a hexagonal array. It is required that the total thrust vector of the operating units has to be directed to the center of mass of the spacecraft. The failure of one of the 3 operating thrusters can be compensated by the 3 thrusters in stand-by. If the second one is failing the mission can be continued either with 2 thrusters only (in case A that both failing thrusters are located side on side) taking $\frac{2}{3}$ of the total power input or using 4 thrusters (in case B that both inoperative thrusters are located at opposite sides) operating each of them with reduced power. If the third thruster fails the propulsion module breaks down totally in case A, whereas in case B still 2 thrusters can operate. Here the total system breaks down if the fourth thruster fails.

The effectiveness of such an electric propulsion module is very high. Even if no thruster would break down, this array gives a duplication of the lifetime looking for missions with longer flight times.

References

[1] Kleber, P. et al., "Konzeptdefinitionsstudie SELAM, solarelektrisches Antriebsmodul," BMBW-Contract RV1-07/9 (624/10)/69, Dec. 1969, Messerschmitt-Bölkow-Blohm GmbH, München-Ottobrunn, W. Germany.

[2] Kruse, H. et al., "Konzeptdefinitionsstudie für ein flugerprobungsfähiges solarelektrisches Antriebsmodul SELAM," BMBW-Contract RV1-07/8/69, Dec. 31, 1969, ERNO-Raumfahrttechnik GmbH, Bremen, W. Germany.

[3] Rasch, W. et al., "Einsatzmöglichkeiten einer nuklearen Energieversorgungsanlage in der Raumfahrt, insbesondere für die Fernsehdirektübertragung," Forschungsbericht W 70-16, April 1970, Bundesministerium für Bildung und Wissenschaft, Bonn, W. Germany.

[4] Au, G. F., *Elektrische Antriebe von Raumfahrzeugen*, G. Braun, Karlsruhe, W. Germany, 1968, pp. 599–627.

[5] Oldekop, W., Rasch, W., Scharf, W., "Vergleichende Betrachtung über den wirtschaftlichen Transport von Großsatelliten für Direkt-Fernsehen in die 24-h-Bahn," *Luftfahrttechnik-Raumfahrttechnik*, Vol. 14, No. 7/8, July/Aug. 1968, pp. 180–185.

[6] Au, G. F., "Electrostatic Propulsion and Mission Analysis in the Federal Republic of Germany," AIAA Paper 69-288, Williamsburg, Va., 1969.

[7] Kaufman, H. R., "An Ion Rocket with an Electron-Bombardment Ion Source," TN D-585, Jan. 1961, NASA.

[8] Kerslake, W. R. et al., "SERT II Experimental Thrustor System," AIAA Paper 67-700, Colorado Springs, Colo., 1967.

[9] Kleinkauf, W., "Energieaufbereitung einer Solarzellenanlage für das Ionentriebwerk ESKA-18-P," *Forschungsbericht* (will be published), Deutsche Luft- und Raumfahrt (DLR) DFVLR, Braunschweig, W. Germany.

[10] Arlt, H. J., Au, G. F., and Baumgarth, S., "Kaufman Ion Thruster of the DFVLR Braunschweig," The 9th International Aeronautical Congress, Paris, June 1969, AFITAE-preprint, pp. 1–26.

[11] Arlt, H. J., Au, G. F., and Baumgarth, S., "Experimentelle Ergebnisse über das Ionentriebwerk ESKA-18," *Raumfahrtforschung*, Band XIII, Heft 5, Sept./Oct. 1969, pp. 197–204.

[12] Ward, J. W. and King, H. J., "Mercury Hollow Cathode Plasma Bridge Neutralizers," *Journal of Spacecraft and Rockets*, Vol. 5, No. 10, Oct. 1968, pp. 1161–1169.

[13] Csiky, G. A., "Langmuir Probe Measurements in a Discharge from a Hollow Cathode," *Journal of Spacecraft and Rockets*, Vol. 7, No. 4, April 1970, pp. 474–475.

[14] Bahr, A., "Plasmabrückenneutralisator," *Jahresbericht 1968 of the DFL*, pp. 99; also "Hohlkathode," *Jahresbericht 1969 of the DFVLR*, pp. 256–257, DFVLR, Braunschweig, W. Germany.

[15] Flügge, S., "*Handbuch der Physik*," Vol. 22, Springer, Berlin-Göttingen-Heidelberg, 1956, pp. 419–420.

[16] Cooper, D. W. and Kuhns, P. W., "Measurement of Ion and Electron Densities of Electron-Bombardment Ion-Thruster Beam," TN D-3761, Dec. 1966, NASA.

[17] Freisinger, J. and Löb, H. W., "Auslegungsgrößen von HF-Triebwerken bei Raumtests," DGLR-Symposium Raumfahrtantriebe II, March 22, 1969, Hannover, Germany.

APRIL 1971 J. SPACECRAFT VOL. 8, NO. 4

A Photographic and Analytic Study of Composite Propellant Combustion in an Acceleration Field

P. G. WILLOUGHBY,* C. T. CROWE,† AND K. L. BAKER‡
United Technology Center, Sunnyvale, Calif.

The experimental fact that acceleration of a composite propellant can effect a significant augmentation of the burning rate is well known. However, an adequate physical insight of the responsible phenomena has been lacking. This paper reports the results of photographing a burning metalized composite propellant under acceleration. The photographic details reveal the inertial retention of burning aluminum particles and the subsequent formation and growth of pits in the surface. An analytic model is developed based on the buoyancy of the globule by combustion gases flowing from the pit bottom and the attendant increased heat transfer from the hot particle, through the supporting gas flow to the propellant surface. The model adequately explains the observed trends in acceleration-produced burning-rate augmentation with ballistic and propellant parameters.

Nomenclature

c_s = specific heat of propellant
e = eccentricity
h_v = heat of vaporization
H_v = $c_s(T_s - T_\infty) + h_v$
n = burning rate exponent
P = pressure
Pe,Pr = Peclet and Prandtl numbers, respectively
Q = heat transfer rate
r,r_s = radial coordinate and globule radius, respectively
$\dot{r}$ = burning rate
Re = Reynolds number
T = temperature
v = velocity
w = metal loading
α = acceleration
η = radial distance along the surface
θ = slope of pit wall
λ = separation distance
μ = gas viscosity
φ = angle between acceleration vector and the normal to the propellant surface
ρ = density
σ = surface tension

Subscripts

a = acceleration
c = chamber
e = edge
f = flame
g = gas
∞ = initial
o = static, surface
p = particle
r = radiation
s = surface, propellant
z = normal coordinate

Presented as Paper 69-173 at the AIAA 7th Aerospace Sciences Meeting, New York, January 20–22, 1969; submitted February 19, 1969; revision received August 6, 1970. This study was performed under contract with the Naval Ordnance Systems Command, Contract N00017-67-C-2429. The technical effort was supported and monitored by B. Drimmer. The photographic work was assisted by D. Girroir. L. Mahle, as well as other members of the Physical Sciences Laboratory, ably assisted in the technical effort. The authors wish to extend their appreciation to these people.

* Senior Scientist, Physical Sciences Laboratory.

† Senior Staff Scientist, Physical Sciences Laboratory now Associate Professor, Washington State University.

‡ Senior Scientist, Physical Sciences Laboratory; now with Electro Optics Associates.

Introduction

IT has long been known that spinning an internal-burning solid-propellant rocket motor about its longitudinal axis for directional stability can significantly affect the motor's internal ballistics. Usually the propellant burning rate and attendant chamber pressures are higher than they would be in the identical motor fired under no-spin conditions.[1] The centrifugal acceleration field is undoubtedly responsible for the augmented regression rate, but understanding of the interaction has been lacking. In order to gain some appre-